Fractal-Based Point Processes

2005

Steven Bradley Lowen
Harvard Medical School
McLean Hospital

Malvin Carl Teich
Boston University
Columbia University

WILEY

2

Scaling, Fractals, and Chaos

Georg Cantor (1845–1918), a celebrated German mathematician, founded set theory and recognized the distinction between countably infinite and uncountably infinite sets, such as the sets of rational and real numbers, respectively.

The French mathematician **Henri Poincaré (1854–1912)** established that certain deterministic nonlinear dynamical systems exhibit an acute sensitivity to initial conditions; this characteristic is now recognized as a hallmark of deterministic chaos.

2.1 DIMENSION

The word "dimension," at least among the technically inclined, generally conjures up an image of a familiar elemental shape such as a line or rectangle. These objects have dimensions that correspond to the measurements used to quantify them: meters and square meters, respectively. Table 2.1 presents four representative "Euclidean" objects along with their dimensions (Mandelbrot, 1982).

Object	Measurement	Dimension
Point	meters^0	0
Line	meters^1	1
Square	meters^2	2
Cube	meters^3	3

Table 2.1 Representative objects: measurements and dimensions.

The union of two objects that have a particular dimension is characterized by that same dimension. Thus, any finite number of points retains a dimension of zero, and three squares connected end to end as a whole maintain a dimension of two. What happens to the dimension as we deform the objects, converting a line into a curve, say, or a square into an ellipse? Common sense suggests that the dimension of an object is robust in the face of such manipulations, and topological theory bears this out. A curve in three-dimensional space, such as a helix, maintains a dimension of unity since uncoiling the helix yields a line of that dimension.

The foregoing discussion illustrates a general property: the dimension of an object cannot exceed the dimension of the space in which it resides (the **Euclidian dimension**). An infinite collection of points immediately adjacent to each other yields a curve, and one can generate a circle from the union of all possible points equidistant from a given point. In both cases, the component objects have a dimension smaller than that of the space. However, one can form a square from a collection of smaller squares, and all squares have a dimension of two. These examples lead to another property: the dimension of each member of a group of objects (**the topological dimension**) cannot exceed the dimension of the object formed by their union.

Taken together, the two properties reveal that a collection of objects of a particular dimension, embedded in an object with another dimension, will have an overall dimension that lies between the two. For example, a collection of points (dimension zero) lying within a square (dimension two) can yield a line (dimension one). Yet, a different collection of points could yield a square of smaller size (dimension two), or a single point (dimension zero). In all cases, however, the dimension of the resulting object lies between zero and two inclusive, in accord with the properties set forth above.

2.1.1 Capacity dimension

Although the concept of dimension as discussed above has intuitive appeal, it is important to develop a more rigorous approach for quantifying dimension. We illustrate one measure, initially introduced by Pontrjagin & Schnirelmann (1932), called the **capacity dimension** or **box-counting dimension** (this technique is discussed in more detail in Sec. 3.5.4). Imagine an ellipse (including its interior) in a plane; we know this object has a dimension of two. Suppose we draw a grid over the ellipse and the surrounding region, yielding a collection of square boxes, and then count the number of squares that overlap at least one point in the ellipse. For squares of a given edge size ϵ, we obtain a number $M(\epsilon)$. (The precise value of this number depends on the alignment of the grid with respect to the ellipse, but this fact does not affect the following argument.)

Now repeat the process with squares half the size of the original ones. The number of squares required to cover the ellipse will increase roughly by a factor of four, since four new squares cover one of the original ones. Thus, $M(\epsilon/2) \approx 4M(\epsilon)$. In the limit, as the size of the squares decreases towards zero, we find

$$M(\epsilon) \to C\epsilon^{-2}, \tag{2.1}$$

where the constant C represents the area of the ellipse, and the alignment of the grid does not affect this result. To extract the exponent from Eq. (2.1), we first take the logarithm, which yields a relation linear in the exponent. Dividing by the logarithm of the inverse box size and taking the limit for small boxes yields the desired exponent:

$$\lim_{\epsilon \to 0} \frac{\ln\big[M(\epsilon)\big]}{\ln(1/\epsilon)} = 2, \tag{2.2}$$

which coincides with the dimension of an ellipse. This suggests a general method for obtaining the capacity dimension that will report the correct exponent even when it may not be readily apparent in the functional form of $M(\epsilon)$.

Now suppose that we repeat the process with a curve in a plane. In this case, the number of squares required increases linearly with $1/\epsilon$, whereupon Eq. (2.2) yields a value of unity. Similarly, a finite collection of n points requires no more than n squares, no matter how small ϵ becomes, resulting in a dimension of zero.

In general, the box-counting technique of determining the dimension proceeds by covering the set in question with "boxes," namely cubes, squares, line segments, or other forms, depending on the space within which the shape lies. The relationship between the number of boxes that contain part of the set and the size of those boxes, as the size decreases to zero, determines the capacity dimension D_0 of the set:

$$M(\epsilon) \to C\epsilon^{-D_0}. \tag{2.3}$$

Thus far, the outcome agrees with our intuition about dimension. When applied to fractals, however, we will see that this approach leads to noninteger values, although it is always bounded from above by the Euclidian dimension, and from below by the topological dimension.

2.2 SCALING FUNCTIONS

Fractals turn out to have close connections to the scaling behavior observed in some functions. A function is said to "scale" when shrinking or stretching both axes (by possibly different amounts, neither equal to unity) yields a new graph that coincides with the original. Scaling leads mathematically to power-law[1] dependencies in the scaled quantities, as we now proceed to show.

Consider a function f that depends continuously on the scale s over which we take measurements. Suppose that changing the scale by any factor a effectively changes the function by some other factor $g(a)$, which depends on the factor a but is independent of the original scale s:

$$f(a\mathsf{s}) = g(a)\, f(\mathsf{s}). \tag{2.4}$$

The only nontrivial solution of this scaling equation for real functions and arguments, and for arbitrary a and s, is (see Prob. 2.5)

$$f(\mathsf{s}) = b\, g(\mathsf{s}), \tag{2.5}$$

with

$$g(\mathsf{s}) = \mathsf{s}^c \tag{2.6}$$

for some constants b and c (Lowen & Teich, 1995; Rudin, 1976). Equations (1.1) and (2.3) provide examples of this relationship.

Restricting a to a fixed value in Eq. (2.4) yields a larger set of possible solutions (Shlesinger & West, 1991):

$$g(\mathsf{s}; a) = \mathsf{s}^c \cos[2\pi \ln(\mathsf{s})/\ln(a)]. \tag{2.7}$$

2.3 FRACTALS

The concept of a fractal involves three closely related characteristics, each of which could serve as a definition in its own right. Indeed, a variety of definitions for fractals exist (Mandelbrot, 1982). Furthermore, fractals can be *deterministic* or *random*. They can also be *static*, such as the Icelandic coastline, or arise from a *dynamical process* such as Brownian motion.

First, fractals possess a form of self-scaling: parts of the whole can be made to fit to the whole in some nontrivial way by shifting and stretching. If stretching equally in all directions yields such a fit, then an object is said to be self-similar. If the fit requires anisotropic stretching, then the object is said to be self-affine (Mandelbrot,

[1] Power-law functions have many aliases, including "algebraic," "hyperbolic," and "allometric." When applied to distributions, the term "heavy-tailed" often (but not always) refers to the same functional form.

1982). For deterministic fractals, the fit is exact. Random fractals, in contrast, fit statistically; transformed parts resemble the whole and have similar probabilistic characteristics, although they do not precisely coincide with it. The coast of Iceland, for example, contains similar features over a range of sizes. As illustrated in Fig. 1.1, what would appear to be a simple bay on a large-scale (coarse-grained) map turns into a meandering connection of inlets and other invaginations when displayed more finely. Examining a length of coastline on a map (without intimate knowledge of the particular section under study) does not provide information about the scale of the map despite knowledge of the size of the entire object, in this case Iceland. In contrast, examining of a section of nonfractal object, such as a circle, readily yields the scale in terms of the size of the object.

Second, the statistics that are used to describe fractals scale with the measurement size employed. For example, the length of the east coast of Iceland follows the form of Eqs. (2.5) and (2.6) with an empirical fractal exponent $c \approx -0.30$, as shown in Prob. 1.1. Statistics with power-law forms are thus closely related to fractals. Indeed, we often highlight this connection by presenting various measures using logarithmic axes for both the ordinate and abscissa; power-law functions become straight lines on such doubly logarithmic graphs and their slopes provide the power-law exponents. This characteristic of fractals proves quite useful.

Third, the fractal exponent that corresponds to a particular statistic, one of the generalized dimensions (see Sec. 3.5.4), assumes a noninteger value. As their size decreases, the number of boxes required to cover the Icelandic coastline increases in such a way that the capacity dimension $D_0 \approx 1.30$ (see Secs. 2.1 and 3.5.4). This scaling exponent assumes a noninteger value lying between that of a line ($D_0 = 1$) and that of a plane ($D_0 = 2$).

2.3.1 Fractals, scaling, and long-range dependence

Fractal behavior, such as an object containing smaller copies within itself, can extend down to arbitrarily small sizes in an abstract mathematical construct. However, real-world fractals generally exhibit minimum sizes beyond which fractal behavior is not obeyed. For example, decreasing the length scale used to measure the length of a coastline will eventually lead to a breakdown in scaling behavior. The geological forces at work over kilometer scales differ from those operating over much smaller length scales, leading to different appearances over these smaller lengths. Certainly at a scale corresponding to individual atoms, the emergent features are expected to bear little resemblance to those at macroscopic length scales.

There are also limits at large scales. Fractal behavior can have a maximum scale, one that often corresponds to the size of the fractal object itself. The minimum and maximum scales that bound fractal behavior are known as the **lower cutoff** (or **inner cutoff**) and the **upper cutoff** (or **outer cutoff**), respectively.

Moreover, any data set collected from a real-life physical or biological experiment will perforce have lower and upper cutoffs, corresponding to the resolution limits of the measurement apparatus and the extent of the entire data set, respectively. These lower and upper measurement cutoffs impose limits on observable fractal behavior

that sometimes prove more restrictive than those of the fractal object under study itself. In the case of the Icelandic coastline portrayed in Fig. 1.1, for example, the resolution of the map from which the measurement is constructed (0.694 km), which is determined by the edge length of the minimum pixel size (see Prob. 1.1), imposes a lower cutoff. An upper cutoff is imposed by the size of the island itself.

Generating a point process from a rate (see Chapter 4) necessarily involves some loss of information, and can also set an effective minimum scale. In both the doubly stochastic and integrate-and-reset point processes considered in Chapter 4, for example, fractal features present in the rate process over time scales shorter than the average time between events will be greatly attenuated in the resultant point process.

In a more rigorous mathematical context, fine distinctions are sometimes drawn between fractals and scaling (Flandrin, 1997; Flandrin & Abry, 1999). The term "scaling" is used when both lower and upper cutoffs exist, "fractal" denotes objects for which no small-size cutoff exists, and "long-range dependence" corresponds to the lack of a large-size cutoff.[2] Since essentially all of the applications we consider derive from limited measurements, our discussion might be more properly framed in terms of scaling rather than fractal behavior. Following common usage, however, we generally do not make this distinction. The Lévy dust, considered in Sec. 4.7, and the zero crossings of ordinary and fractional Brownian motion, considered in Sec. 6.1, are the sole exceptions. These two collections of points, which, properly speaking, are not point processes, are fractal in the strict sense of the term.

2.3.2 Monofractals and multifractals

The scaling behavior discussed thus far involves a single stretching or shifting rule, and a single exponent for each statistic. For some objects, the rule and exponents depend on the position within the object, or on the size of the component. Each such object can thus contain a range of fractal behaviors, and is therefore called a **multifractal** (Mandelbrot, 1999; Sornette, 2004). In this context, a simpler fractal object described in our earlier discussions is called a **monofractal**. Although examples of multifractals can be found, in practice relatively few point-process data sets contain sufficient information to accurately characterize their multifractal spectrum.

Perhaps the best method for attempting such a characterization leads to a multifractal spectrum by simulating a number of surrogate data sets with different parameters, and selecting the best fitting parameters as estimates of the multifractal behavior (Roberts & Cronin, 1996). This method yields good accuracy with as few as $N = 100$ points. However, its inherent parametric approach limits its usefulness in general, since the algorithm requires *a priori* knowledge of the form of the mul-

[2] More precisely, a process is said to have long-range dependence when its autocorrelation has an infinite integral (for continuous-time processes) or an infinite sum (for discrete-time processes) (Cox, 1984). Theoretically, a process could have long-range dependence without exhibiting power-law behavior, but this is uncommon.

tifractal spectrum. Indeed, it estimates only two parameters from the data set rather than an arbitrary form for the multifractal spectrum.

Finally, such methods typically require that the point processes themselves, rather than merely the rates of these processes, exhibit (multi)fractal behavior. Such fractal point processes (see Sec. 5.5.1) form an important subclass of the class of fractal-based point processes (see Sec. 5.5) that we explore, but they do not describe a large number of data sets.

As a consequence of these limitations, we concentrate principally on monofractals in this book. Computer network traffic is a notable exception: the availability of extensive, long data records allow a valid multifractal analysis to be carried out (see Sec. 13.3.8).

2.4 EXAMPLES OF FRACTALS

Fractals abound in many fields: **mathematics** (Mandelbrot, 1982; Stoyan & Stoyan, 1994; Peitgen, Jürgens & Saupe, 1997; Barnsley, 2000; Mandelbrot, 2001; Falconer, 2003; West, Bologna, Grigolini & MacLachlan, 2003; Doukhan, 2003); **physics** (Mandelbrot, 1982; Feder, 1988; Schroeder, 1990; Sornette, 2004); **geology** (Turcotte, 1997); **imaging science** (Peitgen & Saupe, 1988; Turner, Blackledge & Andrews, 1998; Flake, 2000); **electronic devices and systems** (Buckingham, 1983; van der Ziel, 1986, 1988; Weissman, 1988; Kogan, 1996); **complex electronic and photonic media** (Berry, 1979; Merlin, Bajema, Clarke, Juang & Bhattacharya, 1985; Kohmoto, Sutherland & Tang, 1987); **materials growth** (Kaye, 1989; Vicsek, 1992); **signal processing** (Flandrin & Abry, 1999); **engineering** (Lévy Véhel, Lutton & Tricot, 1997); **vehicular-traffic behavior** (Musha & Higuchi, 1976; Bovy, 1998); **computer networks** (Mandelbrot, 1965a; Leland, Taqqu, Willinger & Wilson, 1994; Albert, Jeong & Barabási, 1999; Park & Willinger, 2000); **biology and physiology** (Musha, 1981; Turcott & Teich, 1993; Bassingthwaighte, Liebovitch & West, 1994; West & Deering, 1994, 1995; Collins, De Luca, Burrows & Lipsitz, 1995; Turcott & Teich, 1996; Liebovitch, 1998; Vicsek, 2001; Teich, Lowen, Jost, Vibe-Rheymer & Heneghan, 2001; Shimizu, Thurner & Ehrenberger, 2002); **behavior and psychiatry** (Paulus & Geyer, 1992; West & Deering, 1995; Gottschalk, Bauer & Whybrow, 1995; Teicher, Ito, Glod & Barber, 1996; Anderson, Lowen, Renshaw, Maas & Teicher, 1999; Anderson, 2001); **neuroscience** (Verveen, 1960; Evarts, 1964; Musha, Takeuchi & Inoue, 1983; Läuger, 1988; Millhauser, Salpeter & Oswald, 1988; Teich, 1989; Lowen & Teich, 1996a; Teich, Turcott & Siegel, 1996; Teich, Heneghan, Lowen, Ozaki & Kaplan, 1997; Thurner, Lowen, Feurstein, Heneghan, Feichtinger & Teich, 1997; Lowen, Cash, Poo & Teich, 1997b); fractals also play important roles in **other fields**.

We proceed to consider four examples of fractals, one each of the possible combinations of

- *artificial* and *natural*
- *deterministic* and *random*.

2.4.1 Cantor set

The **Cantor set**, discovered by Georg Cantor (1883), provides an example of an artificial, deterministic, one-dimensional fractal structure that extends to arbitrarily small scales. One particular mathematical construction of this set has as its starting point the closed unit interval

$$\mathcal{C}_0 \equiv [0, 1]. \tag{2.8}$$

From $\mathcal{C}_0$, we form $\mathcal{C}_1$, the next step in the formation of the triadic Cantor set, by removing the middle third of this interval:

$$\mathcal{C}_1 \equiv \left[\tfrac{0}{3}\,,\,\tfrac{1}{3}\right] \bigcup \left[\tfrac{2}{3}\,,\,\tfrac{3}{3}\right], \tag{2.9}$$

where $\cup$ represents the set union operation. We then obtain $\mathcal{C}_2$ from $\mathcal{C}_1$ by removing the middle thirds of *both* segments, so that

$$\mathcal{C}_2 \equiv \left[\tfrac{0}{9}\,,\,\tfrac{1}{9}\right] \bigcup \left[\tfrac{2}{9}\,,\,\tfrac{3}{9}\right] \bigcup \left[\tfrac{6}{9}\,,\,\tfrac{7}{9}\right] \bigcup \left[\tfrac{8}{9}\,,\,\tfrac{9}{9}\right]. \tag{2.10}$$

The set $\mathcal{C}_n$ denotes the nth stage in this process. This procedure is continued indefinitely, leading to the Cantor set itself, $\mathcal{C}$, which is defined as the limit

$$\mathcal{C} \equiv \lim_{n\to\infty} \mathcal{C}_n. \tag{2.11}$$

Fig. 2.1 The first six stages in the construction of a triadic Cantor set. The process begins with the unit interval; removing the middle third of each segment at a given stage yields the following stage. Continuing this process indefinitely yields the Cantor set itself as a limit.

The first six stages in the construction of a triadic Cantor set are displayed in Fig. 2.1. The Cantor set $\mathcal{C}$ consists of two exact copies of itself, in the intervals $\left[0, \frac{1}{3}\right]$ and $\left[\frac{2}{3}, 1\right]$, respectively, each of which is one-third the size of the whole. It also contains four copies of itself, each one-ninth the size of the whole. In fact it has 2^n copies, each 3^{-n} the size of the original set, for all nonnegative integers n. For the triadic Cantor set, increasing the length scale ϵ by a factor of 3 decreases the number of copies $N(\epsilon)$ by a factor of 2, so that $N(\epsilon) \sim \epsilon^{-D_0}$ with $D_0 \equiv \log(2)/\log(3) \doteq$

0.630930. There is, in fact, an entire family of generalized dimensions D_q (see Sec. 3.5.4) but for monofractals such as the Cantor set, these all coincide so that $D_q = D$ for all q.

A set with infinitely many copies of itself, each of vanishing size, can exhibit counterintuitive properties. Such seeming paradoxes often occur in the study of abstract fractals, and we now proceed to examine one in the light of the Cantor set: this set has a total length of zero, but just as many points as the unit interval employed as the first stage in its construction. To show this, we begin with the total length of the Cantor set. The initial stage of the Cantor set consists of the unit interval, and therefore has a Lebesgue measure or length $\mathcal{L}(\mathcal{C}_0)$ of unity. The second stage has 2 segments of length $\frac{1}{3}$, for a total length $\mathcal{L}(\mathcal{C}_1) = \frac{2}{3}$; the nth stage comprises 2^n segments each of length $1/3^n$, yielding $\mathcal{L}(\mathcal{C}_n) = (\frac{2}{3})^n$. Continuing this process indefinitely leads to the total length of the Cantor set itself as a limit:

$$\mathcal{L}(\mathcal{C}) = \lim_{n\to\infty} \mathcal{L}(\mathcal{C}_n) = \lim_{n\to\infty} \left(\tfrac{2}{3}\right)^n = 0. \tag{2.12}$$

So the Cantor set has zero total length.

Turning now to the number of points in the Cantor set, consider a ternary expansion of the points in the original interval $\mathcal{C}_0 \equiv [0, 1]$. Each point x in this interval may be represented by a corresponding sequence of digits $0.a_1a_2a_3a_4\ldots$, where

$$x = \sum_k a_k \left(\tfrac{1}{3}\right)^k, \tag{2.13}$$

with each a_k either 0, 1 or 2. Points of $\mathcal{C}_0$ contained in the open interval $\left(\frac{1}{3}, \frac{2}{3}\right)$ will not appear in $\mathcal{C}_1$, and all have a 1 in the first position after the decimal point of their ternary expansions. (The point $\frac{1}{3}$, the upper limit of the first segment, also has a 1 in the first position, but remains in $\mathcal{C}_1$ and in $\mathcal{C}$ as well. We will return to the issue of endpoints shortly.) Points with a 1 in the second position after the decimal point correspond to the middle third of both segments of $\mathcal{C}_1$, and will not appear in $\mathcal{C}_2$ or in subsequent stages. Thus, $\mathcal{C}_n$ contains only those points without a 1 in any of the first n positions of the corresponding expansions.

In the limit, then, the Cantor set $\mathcal{C}$ contains only those points that do not display a 1 in *any* position of the corresponding expansion; the ternary expansion of any point in $\mathcal{C}$ consists solely of the symbols 0 and 2. For example, the point corresponding to the expansion $0.020202\ldots$ (base 3) $= \frac{1}{4}$ belongs to $\mathcal{C}$, whereas $0.111111\ldots$ (base 3) $= \frac{1}{2}$ does not. Points in the original interval $\mathcal{C}_0$ may also be expanded in *binary* format, with each digit chosen from the set $\{0, 1\}$. Therefore, there exists a one-to-one mapping between the points in the Cantor set $\mathcal{C}$ and those in the original unit interval $\mathcal{C}_0$; simply replace the "2" symbols in the ternary expansion for the former with "1" symbols in the binary expansion of the latter. In particular, the Cantor set has uncountably many points. The endpoints, mentioned earlier, form only a countable subset of the Cantor set, and therefore do not change its cardinality.

Variants of the Cantor set described above, in which each stage in the construction removes a fraction of the points removed in constructing the ordinary Cantor set (see, for example, Rana, 1997), are known as **fat Cantor sets**. Consider removing only the

middle $c/3^n$ of the segments employed in the construction of $\mathcal{C}$, for example, where $0 < c < 1$. Here we remove a total of 2^{n-1} segments of width $c/3^n$ in constructing the nth stage of the fat Cantor set $\mathcal{C}^F$. The total width remaining becomes

$$\begin{aligned}
\mathcal{L}(\mathcal{C}_n^F) &= 1 - \sum_{m=1}^{n} 2^{m-1}\, c/3^m \\
&= \lim_{n\to\infty} \mathcal{L}(\mathcal{C}_n^F) \\
&= \lim_{n\to\infty} \left(1 - \sum_{m=1}^{n} 2^{m-1}\, c/3^m\right) \\
&= 1 - (c/3) \,/\, \left(1 - \tfrac{2}{3}\right) \\
&= 1 - c\,. \qquad (2.14)
\end{aligned}$$

For $c = 1$ we recover the result that $\mathcal{L}(\mathcal{C}) = 0$. The set $\mathcal{C}^F$ therefore has a Lebesgue measure of $1 - c$, but with an uncountably infinite number of points missing when compared with the unit interval $\mathcal{C}_0$. In particular, in this set an infinite number of intervals of infinitesimal size exist near any point that belongs to $\mathcal{C}$. For the Cantor set itself, each point in $\mathcal{C}$ has an infinite number of neighbors in $\mathcal{C}$ that are arbitrarily close to it, but $\mathcal{C}$ lacks intervals of any length.

2.4.2 Brownian motion

We use Brownian motion as an example of an artificial, random fractal. **Brownian motion** has a long and storied history in the annals of several scientific disciplines: biology (Brown, 1828), financial mathematics (Bachelier, 1900), physics (Einstein, 1905; Perrin, 1909), and mathematics (Wiener, 1923; Kolmogorov, 1931; Lévy, 1948). The first observation of this phenomenon appears to have been made in 1785 by Jan Ingenhousz, a Dutch physician, in the course of examining the behavior of powdered charcoal on the surface of alcohol (see Klafter, Shlesinger & Zumofen, 1996, p. 33), but the term Brownian motion arose following the Scottish botanist Robert Brown's (1828) description of the movement of pollen grains in water.

In accordance with general usage, however, we denote as Brownian motion a particular continuous-time random process known as a **Wiener–Lévy process** (Wiener, 1923; Lévy, 1948) [alternate appellations are **Wiener process** (Wiener, 1923) and **Bachelier process** (Bachelier, 1900, 1912)]. Thus, Brownian motion, like the Cantor set, is considered to be an abstract construction, although it does closely approximate much experimental data. Unlike the Cantor set, however, Brownian motion involves randomness in its definition. Different realizations of the Brownian-motion process appear different, although all are governed by the same statistical properties.

One definition of Brownian motion $B(t),\ t \geq 0$, involves the following three properties. First, Brownian motion is a Gaussian process; this signifies that a vector $\{B(t_1), B(t_2),..., B(t_k)\}$ for any positive integer k and any set of times $\{t_1, t_2,..., t_k\}$ has a joint Gaussian (normal) distribution. Second, the mean is zero: $\mathrm{E}[B(t)] = 0$

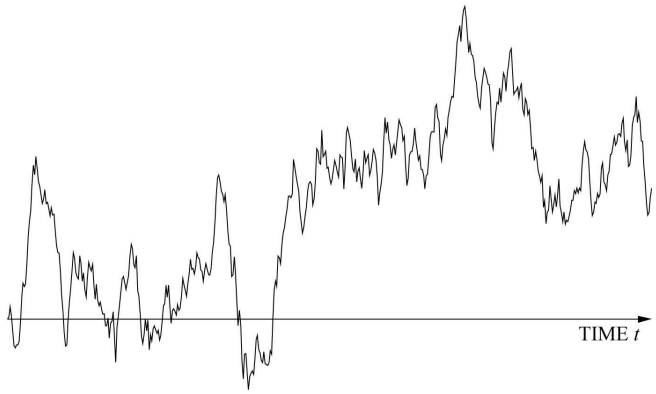

Fig. 2.2 A realization of Brownian motion. Time increases towards the right, with the origin at the left.

for all t, where $\mathrm{E}[\cdot]$ represents expectation or mean. Third, the autocorrelation[3] of the process at two times s and t equals the smaller of the two times

$$\mathrm{E}[B(s)\,B(t)] = \min(s,t) \tag{2.15}$$

for all s and t, where $\min(x,y)$ returns the smaller of x and y. Figure 2.2 displays a realization of Brownian motion.

We can derive a number of other characteristics from these three properties. In particular, Brownian motion contains statistical copies of itself. To see this, define a new function $B^*(t) \equiv B(at)$, a version of Brownian motion with a rescaled time axis. The random process $B^*(t)$ also belongs to the Gaussian family of random processes, with a mean of zero and an autocorrelation

$$\mathrm{E}[B^*(s)\,B^*(t)] = \mathrm{E}[B(as)\,B(at)] = a\min(s,t). \tag{2.16}$$

Now consider rescaling the amplitude of $B^*(t)$: define $B^\dagger(t) = a^{-1/2}\,B^*(t) = a^{-1/2}\,B(at)$. Like $B(t)$ and $B^*(t)$, $B^\dagger(t)$ is a zero-mean Gaussian process. The autocorrelation for $B^\dagger(t)$ is therefore written as

$$\begin{aligned}
\mathrm{E}[B^\dagger(s)\,B^\dagger(t)] &= \mathrm{E}[a^{-1/2}\,B^*(s)\,a^{-1/2}\,B^*(t)] \\
&= a^{-1}\,\mathrm{E}[B(as)\,B(at)] \\
&= a^{-1}\,a\min(s,t) \\
&= \min(s,t),
\end{aligned} \tag{2.17}$$

which is identical to that of the original process $B(t)$.

[3] We define autocorrelation as the expectation of the product of a process at two different times or delays, while autocovariance denotes the result with the mean value removed. For zero-mean processes, the two coincide.

Since $B^{\dagger}(t)$ and $B(t)$ are Gaussian processes with the same mean and autocorrelation, the two processes are statistically identical (Feller, 1971). Thus, changing the time axis by a scale a and the amplitude axis by a scale a^H, with $H = \frac{1}{2}$, yields the same result, and $B(t)$ contains statistical copies of itself at any scale. In Chapter 6 we consider a generalization of Brownian motion, called fractional Brownian motion, in which the parameter H can assume any value between zero and unity.

2.4.3 Fern

We move now from abstract mathematical fractal objects, such as the Cantor set and Brownian motion, to natural fractal objects. These are ubiquitous in the real world. A simple fern provides a particularly clear example. Figure 2.3 displays the main frond of a fern (oriented vertically), which contains many sub-fronds (oriented horizontally), each a miniature copy of the whole.

Fig. 2.3 A fern, an example of a natural fractal with little randomness. The main frond comprises many sub-fronds, each a miniature copy of the whole. This fern, *Athyrium filix-femina* (Lady Fern), was collected from the backyard of the first author's residence in Massachusetts. It is well described as a deterministic fractal.

This scaling continues; each sub-frond contains sub-sub-fronds (oriented vertically again), and at the bottom of the figure there is evidence for a fourth level of detail.

Like all objects in the physical world, ferns have a minimum scale for their fractal behavior, here at the fourth level. The copies, while not perfect replicas of the whole, do not differ much from it; the fern is well described as a deterministic fractal.

2.4.4 Grand Canyon river network

Fig. 2.4 An overhead view of the Grand Canyon, a random natural fractal gouged out by the Colorado river. The main canyon contains many sub-canyons, each resembling the whole in a statistical manner. This photograph was taken from space by astronauts during U.S. Space Shuttle Flight STS61A. Image obtained from: Earth Sciences and Image Analysis, NASA–Johnson Space Center; 15 November 2004; "Astronaut Photography of Earth–Display Record." http://eol.jsc.nasa.gov/scripts/sseop/photo.pl?mission= STS61A&roll=201&frame=75

Whereas a fern provides an example of a deterministic natural fractal, most natural fractals exhibit randomness. Consider the Grand Canyon (Arizona), shown in Fig. 2.4. The main canyon, running from the top left, through the center, and exiting at the lower left, contains a number of sub-canyons along its length. While each sub-canyon appears different from the Grand Canyon itself and from the other sub-canyons, all resemble each other. The sub-canyons resemble the whole in a statistical manner. Again, the scaling continues, with the sub-canyons containing still smaller sub-sub-canyons of similar appearance within them, and so forth, down to the resolution

limit of the photograph. Here the lower limit of fractal behavior derives from the measurement, rather than from the fractal object itself. The Grand Canyon thus provides an example of a random natural fractal.

2.5 EXAMPLES OF NONFRACTALS

Lest the reader gain the mistaken impression that all objects are fractals, we provide four counterexamples, again employing one each of the possible combinations of artificial and natural, and deterministic and random.

2.5.1 Euclidean shapes

Classical Euclidean shapes, such as circles, lines, and simple polyhedra have a single, well-defined scale, and therefore do not exhibit similar behavior over different scales. These artificial, deterministic objects do not reveal further detail upon magnification, nor do they possess copies of themselves. Such shapes are, therefore, not fractal.

2.5.2 Homogeneous Poisson process

Remaining in the abstract realm but turning now to random objects, we consider the one-dimensional homogeneous Poisson process (Parzen, 1962; Cox, 1962; Haight, 1967; Cox & Isham, 1980), perhaps the simplest of all point processes (see Sec. 4.1). Like Brownian motion, different realizations of this process have a different appearance, although each is governed by the same statistical properties. A single constant positive quantity, the rate, denotes the number of events (points) expected to occur in a unit interval, and this quantity completely characterizes the homogeneous Poisson process. The absence of memory completes the definition of this process; given the rate, knowledge of the entire history and future of a given realization of a homogeneous Poisson process yields no additional information about the behavior of the process at the present.

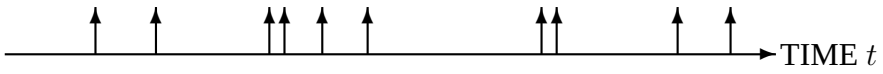

Fig. 2.5 Schematic representation of a one-dimensional homogeneous Poisson process. The time axis runs horizontally to the right, and the vertical arrows depict individual events (points) as they occur in time.

A schematic representation of a realization of a one-dimensional homogeneous Poisson process appears in Fig. 2.5. The vertical arrows depict individual events (points) as they occur, while the horizontal axis represents time. Although the intervals between the events vary they are associated with a fixed time scale via the rate parameter, in contrast to a fractal object. In particular, decreasing the time scale used

to display the process yields a more sparse version of the original that appears quite different from it. Unlike a fractal process, it does not appear to be a random copy of the original. Further, the probability density function for the intervals follows an exponential form [see Eq. (4.3)], rather than the power-law form of Eqs. (2.5) and (2.6). Like the Euclidean shapes considered above, the homogeneous Poisson process is not fractal.

2.5.3 Orbits in a two-body system

The path followed by one of the bodies in a two-body orbiting system, such as the earth and the moon,[4] provides an example of a natural, deterministic, nonfractal object. Newtonian physics predicts that the two bodies will orbit about their mutual center of mass along trajectories described by perfect ellipses, and will do so indefinitely (Newton, 1687; Feynman, Leighton & Sands, 1963, vol. I, pp. 7-1–7-8). These orbits have a single scale; they do not exhibit similar behavior over different scales nor do they contain copies of themselves. The paths resemble the abstract Euclidean shapes exemplified in Sec. 2.5.1.

In contrast, the paths traced by planets in systems containing three or more bodies *do* exhibit fractal characteristics. This is particularly evident when the bodies have similar masses and are separated by similar distances. Such systems exhibit deterministic chaos (see Sec. 2.6), and chaotic systems often have fractal movement patterns.

2.5.4 Radioactive decay

Finally, for an example of a natural, random, nonfractal process, we turn to radioactive decay (Feynman et al., 1963, vol. I, pp. 5-3–5-5). A single radioactive atom will decay at some random time in the future, and, while the exact time of decay remains unknowable *a posteriori*, the probability of decay by any specified time is well known. Imagine, now, a collection of identical radioactive atoms, each undergoing decay at a random time. The registrations of these decay events form a random point process. It is associated with a single time constant or scale: the average decay time of the atoms.

The emissions resemble the homogeneous Poisson process presented in Sec. 2.5.2 provided that the observation times are sufficiently smaller than the average decay time (Rutherford & Geiger, 1910). Like the Poisson process, modifying the time scale over which the radioactive decay process is observed results in a qualitatively different process. Moreover, the probability density function for the times between decays does not follow the power-law form of Eqs. (2.5) and (2.6). Radioactive decay is not a fractal process.

[4] For simplicity of exposition we ignore perturbations induced by other celestial bodies and tides, as well as minor relativistic effects.

2.6 DETERMINISTIC CHAOS

Chaos and fractals are not synonymous, although the two concepts are often conflated. Chaos is, of course, an important topic in its own right (Poincaré, 1908; Devaney, 1986; Glass & Mackey, 1988; Moon, 1992; Ott, Sauer & Yorke, 1994; Strogatz, 1994; Schuster, 1995; Alligood, Sauer & Yorke, 1996; Peitgen et al., 1997; Thompson & Stewart, 2002; Ott, 2002). Even though chaos does not play a central role in the treatment of fractals, we compare and contrast these two phenomena to clarify their relationship.

Chaos describes the behavior of a deterministic nonlinear dynamical system in the presence of the following three features. First, small changes in the initial state of the system must lead to quite different results at some later time. For two identical systems beginning in slightly different states, the difference between them increases exponentially over time. Poincaré (1908) was the first to allude to this "sensitive dependence on initial conditions".[5] Second, and related to the first, the prediction of system dynamics becomes increasingly more difficult as the time of prediction moves further into the future. And third, an infinite number of unstable periodic orbits exists. With arbitrarily small continual adjustments, the dynamics of the system can be forced to follow any number of periodic paths, although in the absence of such adjustments the dynamics quickly depart from all such orbits. The diversity of behavior offered by a chaotic system has profound consequences. Conrad (1986) has categorized five functional roles that chaos might play in biological systems: search, defense, maintenance, cross-level effects, and dissipation of disturbance.

Given a dynamical system, it is customary to plot the state variables in phase space, collapsing the time information in the process. The resulting graph provides a window on the dynamics of the system. For dissipative systems, after an initial transient period system activity converges to a restricted region of phase space called the attractor of the system.

Some systems have **fractal attractors**, also known as **strange attractors**. The dynamics such systems display a rich pattern in phase space; enlarging a section of such an attractor continues to reveal new details without limit. Many (but not all) systems exhibiting chaos have strange attractors. Similarly, many (but not all) strange attractors derive from systems that are chaotic. However, neither feature necessarily implies the other. Unfortunately, the literature is rife with misconceptions pertaining to this issue.

We proceed to demonstrate the fundamental distinction between the two concepts by presenting examples of all four possibilities: chaotic and nonchaotic systems with both fractal and nonfractal attractors. To facilitate comparison between the various systems we confine ourselves to the simple class of iterated-function systems, which

[5] "A very small cause that escapes our notice has a considerable effect that we cannot fail to see, and we then say that the effect arises from chance . . . but it may happen that small differences in the initial conditions produce very large differences in the final phenomena. A small error in the former then produces a very large error in the latter and prediction becomes impossible . . ."—Poincaré (1908)

follow the form

$$x_{n+1} = f(x_n) \tag{2.18}$$

or

$$\begin{aligned} x_{n+1} &= f(x_n, y_n) \qquad \text{a)} \\ y_{n+1} &= g(x_n, y_n) \qquad \text{b)} \end{aligned} \tag{2.19}$$

for the one- and two-dimensional versions, respectively.

2.6.1 Nonchaotic system with nonfractal attractor

We begin with the logistic map, a particular example of Eq. (2.18) that takes the form of a quadratic recurrence relation,

$$x_{n+1} = f(x_n) = c\,x_n(1 - x_n)\,. \tag{2.20}$$

This function maps the unit interval $[0, 1]$ to itself, and exhibits behavior that varies with the parameter c. It is a discrete version of the logistic equation of fame in ecology (Verhulst, 1845, 1847).

We begin by examining the stability of Eq. (2.20). A fixed point satisfies the equation $x_{n+1} = x_n = x_*$, which yields

$$\begin{aligned} x_* &= f(x_*) \\ &= cx_*(1 - x_*) \\ 0 &= x_*\big[x_* - (1 - 1/c)\big]. \end{aligned} \tag{2.21}$$

Eliminating the degenerate value $x_* = 0$ provides $x_* = 1 - 1/c$ for the remaining fixed point. What happens to values near the fixed point determines its stability; to assess this, we use a test value $x_n = x_* + \epsilon_n$, where ϵ_n is a value much smaller than unity. We then have

$$\begin{aligned} x_{n+1} &= f(x_n) \\ x_* + \epsilon_{n+1} &= f(x_* + \epsilon_n) \\ &= c\,(x_* + \epsilon_n)\,\big[1 - (x_* + \epsilon_n)\big] \\ &= c\,x_*(1 - x_*) + c\,\epsilon_n(1 - 2x_* - \epsilon_n) \\ &= x_* + c\,\epsilon_n(1 - 2x_* - \epsilon_n) \\ \epsilon_{n+1}/\epsilon_n &= c\,(1 - 2x_* - \epsilon_n) \\ &= 2 - c\,(1 + \epsilon_n)\,. \end{aligned} \tag{2.22}$$

For the nonchaotic case, we choose $c = 2$. The fixed point then becomes $x_* = 1 - 1/c = \frac{1}{2}$, whereupon Eq. (2.22) yields $\epsilon_{n+1}/\epsilon_n = -2\epsilon_n$ indicating a rapid (quadratic, in fact) relaxation towards the fixed point. Since the fixed point is stable, the attractor of the system consists of that single point only. Thus, a plot of all possible values x_n, after transient effects have subsided, yields a single point, $x_n = \frac{1}{2}$. This zero-dimensional object has no fractal qualities whatsoever, and forms a nonfractal (non-strange) attractor. Furthermore, since all values of x_n converge rapidly to the fixed

point x_*, any differences among starting values must decrease, rather than increase, over time, thereby precluding a sensitive dependence on initial conditions. The system of Eq. (2.20) with $c = 2$ therefore does not exhibit chaos. Figure 2.6 displays this convergence by showing the sequence $\{x_n\}$ that results from two different starting values, $x_0 = 0.1$ and 0.4, and illustrates the lack of chaos in this system.

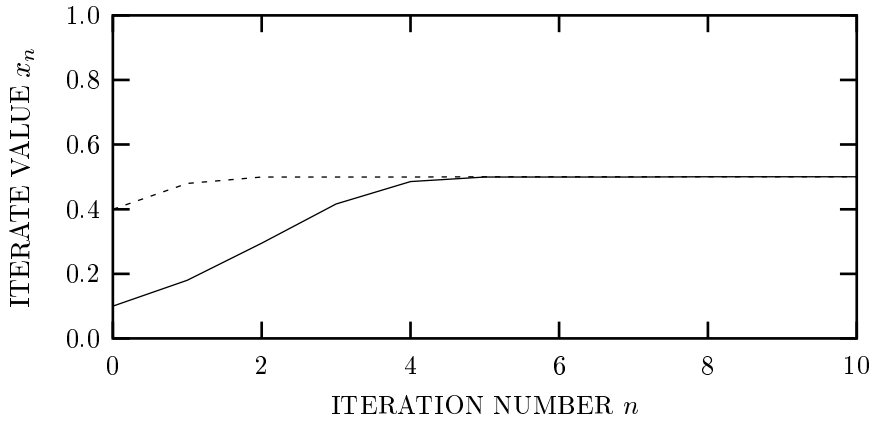

Fig. 2.6 Time course of a logistic system with parameter $c = 2$, for two different starting values: $x_0 = 0.1$ and 0.4. Although the two initial points differ widely, they both converge to the same value, the fixed point $x_* = \frac{1}{2}$. This system thus does not display sensitive dependence to initial conditions, and does not exhibit chaos.

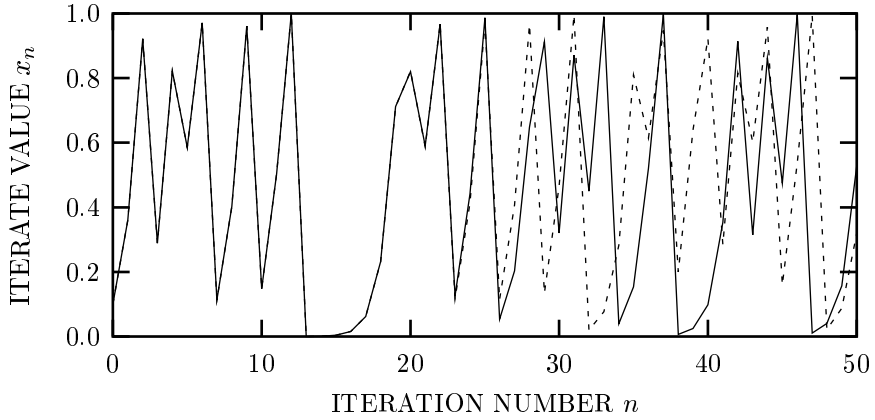

Fig. 2.7 Time course of a logistic system with parameter $c = 4$, for two different starting values: $x_0 = 0.1$ and $0.1 + 10^{-9}$. Although the two initial points differ only slightly, the iterates diverge and are completely unrelated after 30 iterations. This system does indeed display sensitive dependence to initial conditions, and exhibits chaos.

2.6.2 Chaotic system with nonfractal attractor

For the purposes of this example, we again consider the logistic map of Eq. (2.20), but now with $c = 4$. The nonzero fixed point becomes $x_* = 1 - 1/c = \frac{3}{4}$. The stability analysis of Eq. (2.22) now yields $\epsilon_{n+1}/\epsilon_n = -2 - 4\epsilon_n \approx -2$ so that deviations about the fixed point double in magnitude with each iteration. This fixed point thus does not comprise the attractor. In fact, for this value of c no limit cycles exist of any finite period and the entire interval $0 < x_n < 1$ forms the attractor (Schroeder, 1990, pp. 291–294). Except for a set of measure zero, iterates of any initial value x_0 will eventually come arbitrarily close to any specified value in the unit interval. This attractor forms a simple line segment and again has no fractal properties, establishing that for the logistic map with $c = 4$ the attractor is nonfractal.

Despite not having a fractal attractor, the system nevertheless displays chaos (Schroeder, 1990, pp. 291–294). The lack of fixed points or limit cycles suggests this, but a graphical demonstration illustrates it well. Figure 2.7 presents the sequence of iterations $\{x_n\}$ resulting from two starting values: 0.1 and a value just a bit larger, $0.1 + 10^{-9}$. Although indistinguishable at first, the difference between the two paths grows over time, and by iteration $n = 30$ the two sequences exhibit no relation to each other. This sensitivity to initial conditions illustrates the chaotic nature of the logistic system for the parameter value $c = 4$.

2.6.3 Chaotic system with fractal attractor

We next turn to the Hénon attractor (Hénon, 1976). This two-dimensional iterated-function system follows the form of Eq. (2.19) with

$$\begin{aligned} x_{n+1} &= 1.0 + ax_n^2 + by_n \qquad \text{a)} \\ y_{n+1} &= x_n, \qquad\qquad\qquad\quad \text{b)} \end{aligned} \tag{2.23}$$

with $a = -1.4$ and $b = 0.3$. We first establish the fractal nature of the attractor by simulation. Starting with $(x_0, y_0) = (1.08003, 0.305372)$, we iterate Eq. (2.23) 1 000 times, discarding these first results to eliminate any transient behavior, and then iterate a further 3 000 times and retain these values. Figure 2.8a) illustrates the attractor, which forms a boomerang shape bounded by $-1.3 < x, y < 1.3$. The initial pair $(x_0, y_0) = (1.08003, 0.305372)$ belongs to the attractor, as verified by further iterations, justifying its choice as a starting value. Enlarging a small section of Fig. 2.8a) (the box shown at the upper right) yields a banded structure [panel b)]; further enlargements yield substantially similar forms, as shown in panels c) and d). This self-similarity provides evidence of fractal characteristics, and in fact this attractor is indeed a fractal object (Peitgen et al., 1997).

We now proceed to consider the chaotic nature of the Hénon system. As before, we employ two different starting values, $(x_0, y_0) = (1.08003, 0.305372)$, as in Fig. 2.8, and $(x_0 + \epsilon_x, y_0)$ with $\epsilon_x = 10^{-7}$. Figure 2.9 shows the x values of the iterates diverging so that by $n = 43$ the two sequences have essentially no connection to each other, despite being almost identical at $n = 0$; the results resemble those for the logistic system with $c = 4$, displayed in Fig. 2.7.

This establishes the sensitivity to initial conditions of the system, and thereby provides evidence of chaos. More detailed and rigorous analysis supports this conclusion (Peitgen et al., 1997).

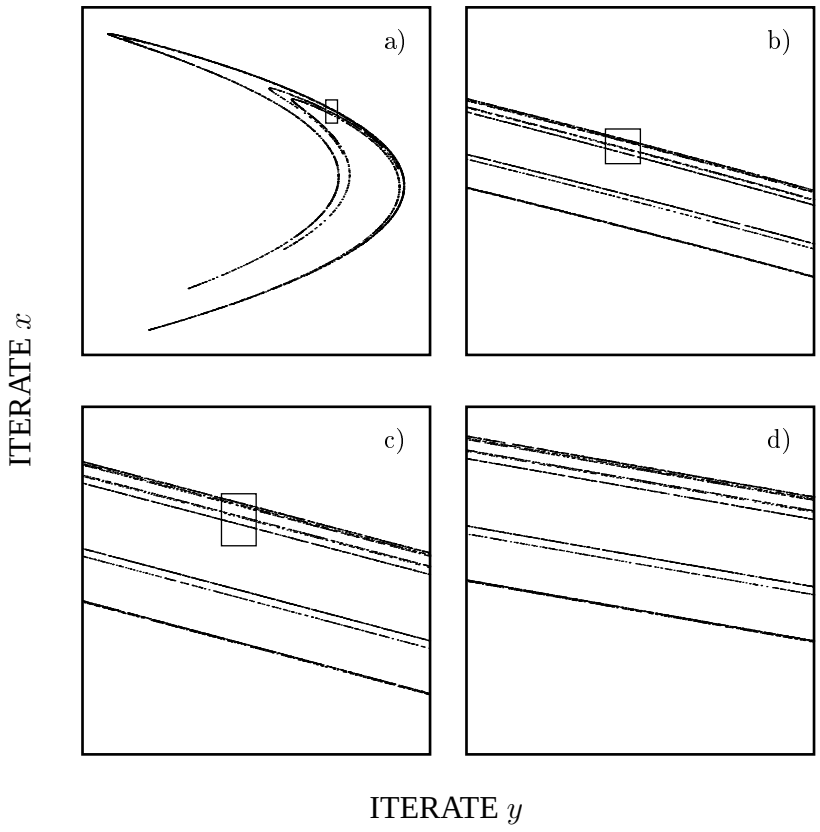

Fig. 2.8 a) Three thousand x-y pairs in the attractor of the Hénon system as shown in Eq. (2.23), with $a = -1.4$ and $b = 0.3$. An initial 1 000 iterations were discarded to eliminate transient effects. b) An enlargement of the small area within the box in panel a): 3 000 values of the attractor constrained to lie in the region $0.6 \leq x \leq 0.7$ and $0.5 \leq y \leq 0.7$. A parallel banded structure emerges. c) A further enlargement, of the area within the box in panel b): 3 000 values within $0.64 \leq x \leq 0.65$ and $0.61 \leq y \leq 0.63$. An enlargement of the upper band in panel b) yields a result similar to panel b). d) A final enlargement of the area within the box in panel c): 3 000 values within $0.644 \leq x \leq 0.645$ and $0.622 \leq y \leq 0.625$. The upper band in panel c) resolves into the same pattern as seen in the whole of panels b) and c). Hence, the attractor has similar structures over many spatial scales, suggesting that it forms a fractal object. This system is also chaotic, as illustrated by the time course displayed in Fig. 2.9.

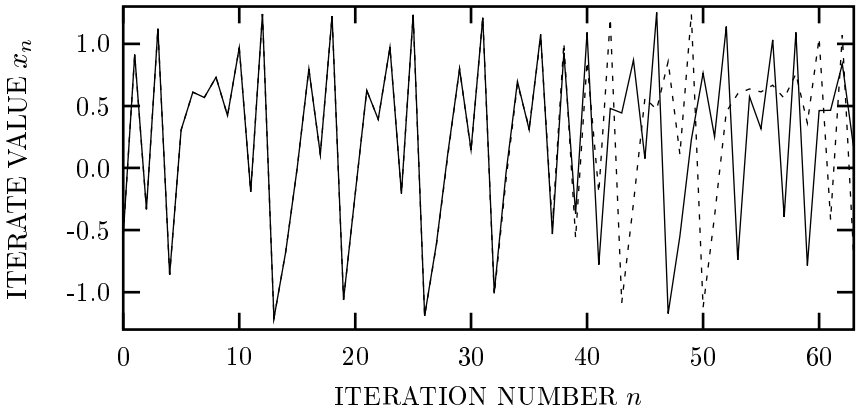

Fig. 2.9 Time course of the Hénon system with parameters $a = -1.4$ and $b = 0.3$, for two different starting values: $(x_0, y_0) = (1.08003, 0.305372)$, and $(x_0 + \epsilon_x, y_0)$ with $\epsilon_x = 10^{-7}$. Again, although the two initial points differ only slightly, the iterates diverge and appear completely unrelated by the 43 iteration. Like the logistic system with $c = 4$ (see Fig. 2.7), this system displays sensitive dependence to initial conditions, and exhibits chaos. The attractor for this system is fractal, however, as illustrated in Fig. 2.8.

2.6.4 Nonchaotic system with fractal attractor

Finally we consider a nonchaotic system which nevertheless has an attractor with fractal characteristics. We again employ the logistic map, Eq. (2.20), with the parameter $c \doteq 3.56995168804$. As previously, we begin by simulating the system to illustrate the fractal nature of the resulting attractor. Using an arbitrary starting value $x_0 = 0.31412577217182861803$, we iterate Eq. (2.20) 3 000 times after discarding the first 1 000 iterates.

The attractor is illustrated in Fig. 2.10a) — it forms a set of disconnected regions in the unit interval $0 < x < 1$. Progressive enlargements of regions of the x-axis of Fig. 2.10a) (delineated by the horizontal lines portrayed in the top three panels) yield new detail. Although different in form from that of the Hénon attractor, the evident self-similarity suggests that the attractor is fractal.

Moving now to confirm the presence or absence of chaos in this system, we again employ two different starting values: $x_0 = 0.87951016911829671$ and $x_0 = 0.89087022021791951$, chosen from the values shown in Fig. 2.10a), after 1 000 iterations to eliminate transient effects. As shown in Fig. 2.11, unlike the results for the logistic system with $c = 4$ and for the Hénon system, different starting points do not diverge. The system of Eq. (2.20) with $c \doteq 3.56995168804$ therefore does not exhibit sensitive dependence on initial conditions and is not chaotic. Other mathematical models of nonchaotic systems with fractal attractors have been set forth (Grebogi, Ott, Pelikan & Yorke, 1984), as has a physical experiment exhibiting such behavior (Ditto, Spano, Savage, Rauseo, Heagy & Ott, 1990).

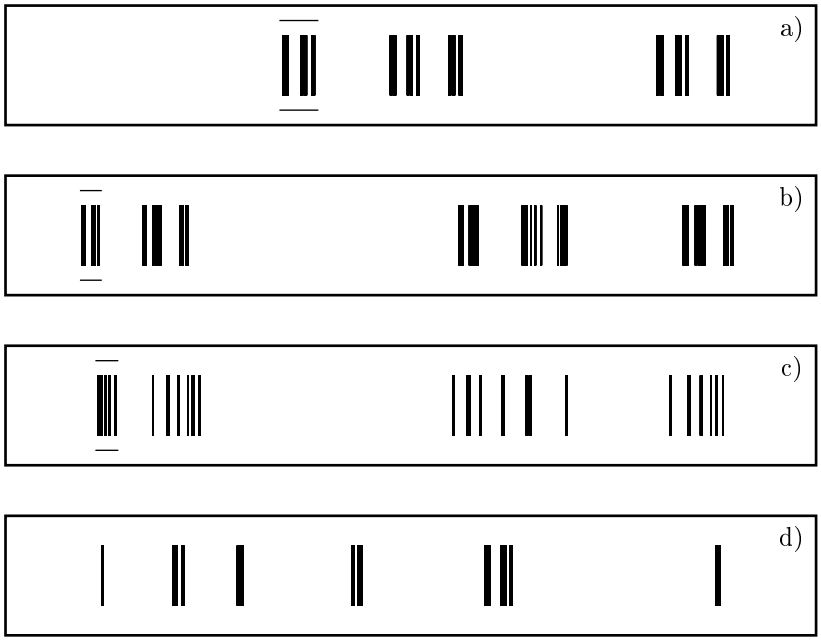

Fig. 2.10 a) Three thousand values in the attractor of the logistic system [Eq. (2.20)] with parameter $c \doteq 3.56995168804$. An initial 1 000 iterations were discarded to eliminate transient effects. Each iterate is represented by a vertical line for clarity. The x axis ranges from zero to unity in this panel. Horizontal lines above and below the left-most cluster delineate the interval enlarged in the subsequent panel. b) An enlargement of the original interval delineated by the horizontal lines in panel a): 3 000 values of the attractor constrained to lie in the region $0.338 \leq x \leq 0.386$. Increased detail emerges with a structure similar to that of the whole attractor in a). c) and d) Further enlargements of the regions delineated by horizontal lines in the preceding panels: 3 000 values of the attractor in the intervals $0.3424 \leq x \leq 0.3437$ and $0.342544 \leq x \leq 0.342581$, respectively. Fresh new structures that resemble those in panels a) and b) continue to appear, suggesting that the attractor is fractal. This system is not chaotic, however, as revealed by the time course displayed in Fig. 2.11.

2.6.5 Chaos in context

Considering the results presented to this point, we see that systems can exhibit chaotic behavior or fractal (strange) attractors, or both, or neither. All four possibilities exist.

From a fundamental perspective, the term chaos describes certain nonlinear deterministic dynamical *systems* whereas the term fractal describes certain *objects*. Thus, chaos does not imply fractal nor does fractal imply chaos.

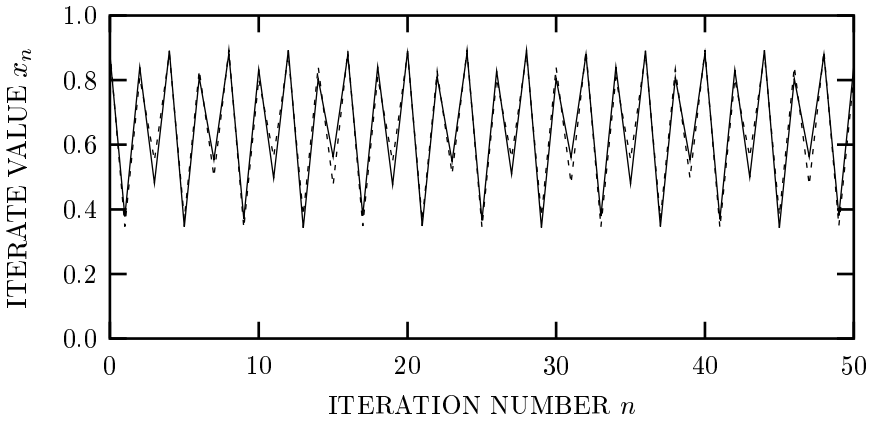

Fig. 2.11 Time course of the logistic system of Eq. (2.20) with parameter $c \doteq 3.56995168804$, for two different starting values. The iterated values maintain a difference roughly equal to that of the starting values, ≈ 0.01, neither converging nor diverging. Hence, this system does not display sensitive dependence to initial conditions, and does not exhibit chaos. The attractor for this system is fractal, however, as illustrated in Fig. 2.10.

Moreover, the presence of significant noise or random behavior in a system generally precludes a meaningful assertion that the system is chaotic. Noise experiences the amplifying behavior of the system's sensitivity to initial conditions, so that even identical starting values experience rapidly diverging paths. Under such conditions, the concept of chaos loses its usefulness. Instead, the random nature of the system, imparted by the noise, becomes a key defining quality of its dynamics.

Since the topic of this treatise is random fractals, we do not consider chaos further.

2.7 ORIGINS OF FRACTAL BEHAVIOR

2.7.1 Fractals and power-law behavior

Why are fractal characteristics found in so many systems, both natural and synthetic? A good part of the reason turns out to be the close connection between fractals and scaling and hence between fractals and power-law behavior (see Secs. 2.2 and 2.3). Indeed, close examination reveals that the fractal behavior associated with many of the models considered throughout this book derives explicitly from the power-law relationships embodied in these models. When no such direct link exists, it turns out that other intrinsic properties of these models ultimately lead to power-law relationships. Power-law relationships can sometimes be traced to the presence of a cascade process in the underlying phenomenon.

The essential notion of a fractal has historical antecedents in theory and experiment alike (see Mandelbrot, 1982, Chapter 41). Consider Leibniz's (1646–1716) conception of fractional integro-differentiation and his definition of the straight line; Kant's (1724–1804) ruminations about the lack of homogeneity in the distribution of matter; Laplace's (1749–1827) suggestion that the scaling nature of Newton's Law of gravitation offered an axiom more natural than that of Euclid; and Weierstraß's (1815–1897) construction of a continuous, but nowhere differentiable, function.

In the empirical domain, we recall Weber's (1835) finding that the relaxation of a stretched silk thread follows a decaying power-law function of time, and Kohlrausch's (1854) observation that the decay of charge in a Leyden jar follows this very same form. We appreciate that Omori (1895) long ago recognized that the rate of aftershocks following an earthquake decays as an inverse function of time.

Indeed, power-law behavior is ubiquitous (see, for example, Malamud, 2004). It occurs in many guises, including deterministic laws, first-order statistics, second-order statistics, distributions, and nonlinear transformations. It is observed in the dynamical responses of systems and in their frequency spectra. Pareto (1896) long ago discovered that scale-invariant, power-law distributions characterize the income of individuals in many societies.[6] Behavior in accord with the **Pareto distribution**,[7] and its discrete counterpart, the **zeta distribution**, emerges in a broad array of contexts. Examples include:

- The number of species in different genera (Willis, 1922).
- The number of publications by different authors (Lotka, 1926).
- The agricultural yields of different sized plots (Fairfield-Smith, 1938).
- The energies of earthquake occurrences (Gutenberg & Richter, 1944).
- The mass densities of yarns of different lengths (Cox, 1948).
- The frequencies of word usage in natural languages (Zipf, 1949).
- The sizes of computer files (Park, Kim & Crovella, 1996).

The question posed at the beginning of this section — "Why are fractal characteristics found in so many systems?" — can thus be recast as: "Why is power-law behavior found in so many systems?"

2.7.2 Physical laws

Several key laws of classical physics take the form of deterministic power-law functions of the distance r,

$$F \propto r^{c}, \tag{2.24}$$

[6] A photograph of Pareto stands at the beginning of Chapter 7.
[7] A useful generalization of the Pareto distribution has been provided by Mandelbrot (1960, 1982), as will be elaborated subsequently.

where F is the force (or field) and r is the distance (see Feynman, 1965). Perhaps the most prominent example of this scaling relation is Newton's (1687) Law of gravitation, which provides that the gravitational field F associated with an object at a distance r follows an inverse-square law, $\mathsf{F} \propto \mathsf{r}^{-2}$, so that $c = -2$.

The Coulomb field associated with a charged particle also behaves in accordance with Eq. (2.24), again with $c = -2$. Other charge configurations similarly lead to power laws, but with different exponents; examples are an infinite line of charge ($c = -1$); a charge dipole ($c = -3$); a charge quadrupole ($c = -4$); and the van der Waals force between a pair of dipoles ($c = -7$). In the study of the mechanics of materials, Hooke's Law provides that the restoring force for an elastic medium also obeys Eq. (2.24), where r is the deformation and $c = +1$ (see Gere, 2001). Also, the Langmuir–Childs Law for space-charge-limited current flow in electronic devices dictates that $\mathsf{i} \propto V^{3/2}$, where i is the current and V is the voltage (see Terman, 1947, Sec. 5–5).

Some physical processes are conveniently described in terms of power-law functions of time, as evidenced by the following examples: (1) the distance d traveled by an object falling under the force of gravity is characterized by $d \propto t^2$; (2) Kepler's Third Law of celestial mechanics specifies that the major axis b of an elliptical planetary orbit is related to the orbital period T via $\mathsf{b} \propto \mathsf{T}^{2/3}$; and (3) the time course of the mean photon flux density emitted by a charged particle via Čerenkov radiation varies as $h(t) \propto t^{-5}$ (see Prob. 10.6).

In quantum mechanics, the allowed energy levels E_{j} of many systems are proportional to some power of the quantum number j (see Saleh & Teich, 1991, Chapter 12),

$$E_{\mathsf{j}} \propto \mathsf{j}^{\,c}. \tag{2.25}$$

Examples are the hydrogen atom ($c = -2$); the harmonic oscillator with a linear restoring force ($c = +1$); the anharmonic oscillator with a cubic restoring force ($c = +\frac{4}{3}$); and the infinite quantum well ($c = +2$). The rigid rotor behaves as $E_{\mathsf{j}} \propto \mathsf{j}\,(\mathsf{j}+1)$. The spatial scaling of the Lagrangian for these systems allows us to deduce these exponents directly from the form of the potential energy function (see Schroeder, 1990, pp. 66–67).

For simple physical systems, the exponents c are typically integers or rational numbers, although fractional exponents are not uncommon in semiconductor physics (see Saleh & Teich, 1991, Chapter 15). In the biological sciences, fractional exponents are more the rule than the exception, as will become apparent subsequently.

2.7.3 Diffusion

In the domain of stochastic processes, diffusion offers a straightforward route to achieving power-law dynamics (Whittle, 1962; Marinari, Parisi, Ruelle & Widney, 1983). In one-dimensional diffusion, an object moves randomly along an axis, with no preferred direction, and with motion at each instant that is independent of motion at all other times. The path of such an object coincides with Brownian motion, discussed in Sec. 2.4.2. Equation (2.15) shows that the variance of the position grows linearly

with time; given the zero-mean Gaussian nature of the process, this leads immediately to a probability density for the particle position x:

$$p_x(x) = (4\pi\Delta\, t)^{-1/2}\, \exp\left(-\frac{x^2}{4\Delta\, t}\right), \tag{2.26}$$

with Δ a diffusion constant. The peak height of the density decays with time as $t^{-1/2}$, an inverse power law. Given a concentration of small objects u_0 (particles, for example) clustered tightly about a starting value x_0, a simple modification of Eq. (2.26) yields a particle concentration envelope $u(x,t)$ given by

$$u(x,t) = u_0(4\pi\Delta\, t)^{-1/2}\, \exp\left(-\frac{(x-x_0)^2}{4\Delta\, t}\right). \tag{2.27}$$

For **diffusion in a multidimensional Euclidean space** of (integer) dimension D_{E}, the motion along each of the component axes forms an independent realization of Brownian motion. The corresponding concentration profile then becomes (see, for example, Pinsky, 1984)

$$u(\mathbf{x},t) = u_0(4\pi\Delta\, t)^{-D_{\mathrm{E}}/2}\, \exp\left(-\frac{|\mathbf{x}-\mathbf{x}_0|^2}{4\Delta\, t}\right), \tag{2.28}$$

where $\mathbf{x}$ and $\mathbf{x}_0$ represent the general and initial position vectors, respectively. The concentration decays as $t^{-D_{\mathrm{E}}/2}$, providing exponents $\frac{1}{2}$, 1, and $\frac{3}{2}$ for $D_{\mathrm{E}} = 1,\, 2$, and 3, respectively. For diffusion on objects that are physical examples of fractals, the fractal dimension of the object replaces the Euclidean dimension D_{E} in Eq. (2.28), thereby offering a larger set of allowable exponents. Problems 10.8 and 10.9 address the ramifications of such diffusion processes.

Diffusion-limited aggregation (DLA) describes the aggregation and growth of structures when diffusion dominates transport (Witten & Sander, 1981). This model characterizes a broad variety of phenomena including electrodeposition, dielectric breakdown, snowflake formation, mineral-vein formation in geologic structures, and the growth of biological structures such as coral (see, for example, Vicsek, 1992; Halsey, 2000).

Subdiffusion is an important form of anomalous diffusion in which the mean-square displacement varies as t^{α} ($0 < \alpha < 1$) rather than as t (see Bouchaud & Georges, 1990). This process can be understood in a simple way by making use of fractional Gaussian noise (see Sec. 6.2) in a generalized Langevin equation (Kou & Xie, 2004).

2.7.4 Convergence to stable distributions

An important and far-reaching rationale for the emergence of power-law distributions has its origins in the limit theorem developed by Paul Lévy (1937, 1940) (see also Gnedenko & Kolmogorov, 1968; Feller, 1971; Mandelbrot, 1982; Christoph & Wolf, 1992; Samorodnitsky & Taqqu, 1994; Bertoin, 1998; Sato, 1999; Sornette, 2004).

Sums of identical and independent continuous random variables are characterized by **stable distributions**, which generally have power-law tails. The sole exception is the Gaussian distribution (Gauss, 1809), which emerges (via the ordinary central limit theorem) when the constituent random variables are endowed with finite second moments.[8]

Discrete analogs of the family of continuous stable distributions have recently been examined (Hopcraft, Jakeman & Tanner, 1999; Matthews, Hopcraft & Jakeman, 2003; Hopcraft, Jakeman & Matthews, 2002, 2004). These probability distributions typically follow the form

$$p(n) \sim 1/n^c, \quad 1 < c < 2, \tag{2.29}$$

for large n. They have zero mode and infinite mean in the absence of an upper cutoff. However, for counting distributions with an upper cutoff, and therefore a finite mean, sums converge to the Poisson distribution, which assumes the role played by the Gaussian for the continuous stable distributions.

2.7.5 Lognormal distribution

A closely related rationale for the presence of power-law behavior stems from the features of the **lognormal distribution** (Kolmogorov, 1941; Aitchison & Brown, 1957; Gumbel, 1958). This distribution is often used as a model for characterizing systems comprising products of random variables, via an argument that proceeds as follows. A product of random variables with finite second moments, under logarithmic transformation, becomes a sum. Application of the ordinary central limit theorem renders the sum Gaussian (normal). The original product, then, obeys the lognormal distribution since its logarithm has a normal distribution.

The lognormal distribution has a long tail and sums of independent lognormally distributed random variables retain their lognormal form (Mitchell, 1968; Barakat, 1976); although these sums ultimately do converge to Gaussian form, the convergence is exceedingly slow. Moreover, the tail of the lognormal distribution is closely mimicked by a power-law distribution over a wide range (Montroll & Shlesinger, 1982; Shlesinger, 1987; West & Shlesinger, 1989, 1990); these authors further argue that many data thought to obey an inverse power-law distribution instead obey the lognormal law over a broad range and then ultimately transition to power-law behavior at very large values of the random variable.

In the domain of discrete processes, the Poisson transform of the lognormal distribution has found widespread use in modeling the photon fluctuations of laser light transmitted through random media such as the turbulent atmosphere (Diament & Teich, 1970a; Teich & Rosenberg, 1971). The justification for using the lognormal model here is the same as that provided above: in traveling from source to receiver, the laser light encounters a large number of independent atmospheric layers with random transmittances.

[8] Photographs of Gauss and Lévy can be found at the beginning of Chapter 8. A biographical sketch of Lévy is provided by Mandelbrot (1982, Chapter 40).

2.7.6 Self-organized criticality

Power-law behavior arises in other ways as well. Some systems spontaneously evolve toward a critical state and thereby generate power-law distributions. A sandpile provides the canonical example of this process, called **self-organized criticality** (Bak, Tang & Wiesenfeld, 1987; Bak, 1996), and abbreviated SOC; the addition of grains of sand to the top of a sandpile results in the formation of a cone at exactly the critical angle of repose. Some added grains merely stop where they land, but many trigger avalanches with power-law varying sizes, maintaining the critical state.

Expansion-modification systems provide another example of such spontaneous evolution. In this case, two processes operate simultaneously, one creating long-range correlation, and the other destroying it; the resulting construct exhibits correlations over all scales, and therefore fractal structure (Li, 1991). As an example, each element in a binary sequence is either inverted with probability p, or duplicated with probability $1 - p$. Similar behavior may occur in a variety of artificial and natural systems, as they evolve towards complex, critical states and produce power-law behavior. In a related model, simple white noise perturbs the movement of activated neural clusters and competing dissipative and restorative forces ultimately generate $1/f$-type noise (Usher, Stemmler & Olami, 1995).

As another particular example, a collection of interconnected processes that evolves according to the logistic equation generates power-law-distributed amplitudes over a broad range of system parameters (Solomon & Richmond, 2002).

2.7.7 Highly optimized tolerance

Highly optimized tolerance (Carlson & Doyle, 1999; Doyle & Carlson, 2000; Carlson & Doyle, 2002) suggests another possible origin for power-law behavior. According to this theory, power-law behavior emerges naturally as a result of the evolution of a complex system toward optimal performance and robustness. Natural selection is said to drive the evolution for collections of living organisms, while engineering design provides the optimizing impetus for artificial systems. This evolutionary process leads to the emergence of specialized states (which would be rare in a random system without design input) concomitantly with power-law behavior.

Power-law characteristics, and hence fractal behavior, can therefore emerge naturally from system evolution via a number of different constructs (Gisiger, 2001).

2.7.8 Scale-free networks

Yet another way that power-law behavior comes into play is via **scale-free networks** (Albert & Barabási, 2002; Dorogovtsev & Mendes, 2003; Pastor-Satorras & Vespignani, 2004). For such networks, no node is typical. Some have an enormous number of connections whereas most are only weakly connected to others. Since well-connected nodes, called hubs, can have hundreds, thousands, or millions of links, there is no scale associated with the network. Connectivity in links per node is described by a probability law, known as the **degree distribution**, that typically

follows a power-law form (Krapivsky, Rodgers & Redner, 2001):

$$p(n) \sim 1/n^c, \quad 2 < c < 3.5. \tag{2.30}$$

There are many ways in which scale-free networks can come into being (see, for example, Krapivsky, Redner & Leyvraz, 2000). The underlying features that lead to the formation of such networks are continual development and the preferential attachment to highly linked nodes. As new nodes are formed, the network continues to evolve; each new node tends to connect to the more highly connected existing nodes since these are most easily identified.

Examples of scale-free networks in the biological domain stretch from cellular metabolic networks, in which biochemical reactions link a collection of molecules, to the brain, in which axons and dendrites link a collection of neurons (Eguíluz, Chialvo, Cecchi, Baliki & Apkarian, 2005). Such networks are plentiful in the technological arena: important examples are air transportation systems, the Internet, and the World Wide Web (see Sec. 13.2.1). Scale-free networks are also pervasive in the social domain: examples include scientific collaborations connected by joint publications; scientific papers linked by citations; people connected by professional associations or friendships; epidemics of contagious disease linked by family members; and businesses linked by joint ventures. They have the salutary feature of being robust against accidental failures because random breakdowns selectively affect the most plentiful nodes, which are the least connected. Such networks are, however, highly vulnerable to coordinated attacks directed at the hubs, which are the most intricately connected of the nodes (Albert & Barabási, 2002).

Despite the evident diversity of these scale-free networks, their common architecture brings them under the same mathematical umbrella: the power-law distribution embodied in Eq. (2.30). The range of asymptotic power-law exponents is rather narrow and differs from that for discrete stable distributions [compare Eqs. (2.29) and (2.30)]. The convergence properties of sums of identical, independently distributed discrete zeta random variables that are suitable for characterizing scale-free networks have recently been established. The limiting form turns out to be the Poisson distribution but the convergence can be exceptionally slow (Hopcraft et al., 2004), much as with the convergence of sums of lognormal random variables to Gaussian form (see Sec. 2.7.5). Problems involving discrete scale-invariant behavior should be formulated in terms of discrete models since continuum models and mean-field approximations can lead to erroneous results (Hopcraft et al., 2004).

Not all networks are scale-free, of course. Prominent exceptions include the locations of atoms in a crystal lattice, the U.S. highway system, the power grid in the Western United States, and the neural network of the organism *Caenorhabditis elegans*.

2.7.9 Superposition of relaxation processes

Finally, we note that the observation of first- and second-order statistics with power-law behavior is often ascribed to a **superposition of relaxation processes** exhibiting a spread of time constants. Maxwell's student Hopkinson (1876) appears to have

originated this explanation, suggesting that the power-law decay of the charge in a Leyden jar might be understood on the basis of various relaxation times for the different silicate components of the glass through which the discharge occurred. However, this argument was later abandoned as unworkable because of the large number of exponentials required. von Schweidler (1907) resurrected this approach by considering a large number of relaxation processes with a wide spread of time constants. He noted that the properties of the gamma function were such that a power-law function could be represented in terms of a weighted collection of exponential functions with different relaxation times.

In the context of semiconductor physics, van der Ziel (1950) used a correlation-function version of this approach to explain the inverse-frequency form of the spectrum; Halford (1968) subsequently offered a generalization of this model. This construct finds wide acceptance in the semiconductor-physics community by virtue of its connection to trapping mechanisms, which offer an exceptionally wide range of time constants (McWhorter, 1957, see also Prob. 7.10). Buckingham (1983, Chapter 6) addressed the role of the weighting functions.

Many other materials and systems, physical and biological alike, display similar power-law behavior, as shown in Chapter 5. However, the relaxation-process approach is rarely appropriate for characterizing these processes because of the enormous range of time constants required to yield $1/f$ behavior over a reasonable range of frequencies. A ratio of time constants of 10^6, for example, yields $1/f$ behavior only over four decades of frequency whereas a ratio of 10^{12} offers 10 decades (Buckingham, 1983, Chapter 6; see also Prob. 9.1 and Fig. B.6). Few systems aside from semiconductors offer the requisite range of time constants.

Another way of mitigating the presence of power-law behavior is to assume that an exponential cutoff ultimately prevails. In practice this often turns out not to be the case, however. Indeed, von Schweidler (1907) himself carried out extensive experiments seeking such a cutoff in the decay of charge in Leyden jars, but found none.

2.8 UBIQUITY OF FRACTAL BEHAVIOR

2.8.1 Fractals in mathematics and in the physical sciences

The most comprehensive treatments of fractals have principally been in mathematics and the physical sciences. Extensive treatments have appeared, for example, in the following books: Mandelbrot (1982); Feder (1988); Peitgen & Saupe (1988); Schroeder (1990); Peitgen et al. (1997); Lévy Véhel et al. (1997); Turcotte (1997); Turner et al. (1998); Flandrin & Abry (1999); Flake (2000); Barnsley (2000); Park & Willinger (2000); Mandelbrot (2001); Falconer (2003); West et al. (2003). The application of fractals in fields such as economics, finance, and hydrology is widespread (see, for example, Mandelbrot, 1982, 1997; Mandelbrot & Hudson, 2004; Henry & Zaffaroni, 2003; Montanari, 2003).

Fractal analysis in the physical sciences proves highly important, as indicated by the following examples:

- We are all keenly aware of the fractal geometry of nature, thanks to the seminal work of Benoit Mandelbrot (1982).
- The noise in many electronic components and systems exhibits fractal behavior at low frequencies (Sec. 5.4.1).
- Semiconductor layered structures comprising stacks of materials of different bandgaps have been fabricated in the form of Cantor sets (Cantor, 1883), as well as Fibonacci (1202), Thue–Morse (Thue, 1906, 1912; Morse, 1921b,a), and Rudin–Shapiro (Rudin, 1959; Shapiro, 1951) sequences. Such nonperiodic, deterministic structures can exhibit fractal electronic, thermal, and magnetic properties (see, for example, Merlin et al., 1985; Kohmoto et al., 1987; Kolář, Ali & Nori, 1991; Dulea, Johannson & Riklund, 1992).
- Photonic materials and devices consisting of layers of materials with different refractive indices have also been constructed in the form of Cantor sets, as well as Fibonacci and Thue–Morse sequences (Jaggard & Sun, 1990; Kolář et al., 1991; Liu, 1997; Jaggard, 1997; Zhukovsky, Gaponenko & Lavrinenko, 2001). For example, Hattori, Schneider & Lisboa (2000) suggested constructing a fiber Bragg grating that takes the form of a Cantor set. Such nonperiodic and deterministic photonic media can exhibit optical properties with unusual features, including: (1) optical reflection and transmission with self-similar spectra (Gellermann, Kohmoto, Sutherland & Taylor, 1994; Dal Negro, Oton, Gaburro, Pavesi, Johnson, Lagendijk, Righini, Colocci & Wiersma, 2003; Ghulinyan, Oton, Dal Negro, Pavesi, Sapienza, Colocci & Wiersma, 2005; Dal Negro, Stolfi, Yi, Michel, Duan, Kimerling, LeBlanc & Haavisto, 2004); (2) complex light dispersion (Hattori, Tsurumachi, Kawato & Nakatsuka, 1994); (3) band-edge group-velocity reduction (Dal Negro et al., 2003; Ghulinyan et al., 2005); (4) pseudo-bandgaps and omnidirectional reflection (Dal Negro et al., 2004); and (5) light emission with uncommon spectral characteristics (Dal Negro, Yi, Nguyen, Yi, Michel & Kimerling, 2005).
- Light scattered or refracted by passage through a random fractal phase screen exhibits fractal wave properties (Berry, 1979; Jakeman, 1982); Berry (1979) coined the term **diffractal** to describe the resulting wave.
- Errors in telephone networks often occur as fractal clusters (Prob. 7.7).
- The photon statistics of Čerenkov radiation exhibit fractal characteristics under certain conditions (Prob. 10.6).
- Analysis of the fractal statistics of earthquake patterns can assist in the prediction of future earthquake occurrences (Prob. 10.7).
- Computer communication networks evolve into scale-free forms and the traffic resident on these networks exhibit fractal characteristics (Chapter 13).

2.8.2 Fractals in the neurosciences

There have been fewer comprehensive treatments of fractals in the biological sciences; we explicitly note those of Bassingthwaighte et al. (1994), West & Deering (1995), and Liebovitch (1998). Fractals play an important role in biological sciences such as ecology (see, for example, Halley & Inchausti, 2004), which has often been a breeding ground for novel mathematical approaches.

In this and the following section, respectively, we examine a number of examples of fractal behavior in the neurosciences and in medicine and human behavior.

Power-law behavior is common in the neurosciences. Featured at levels from the molecular to the organism, it is manifested in many systems. Neural systems evidently benefit from the flexibility of being able to match the time scale of a current stimulus while incorporating the memories of past stimuli. We present a number of examples, emphasizing those that fall in the class of fractal-based point processes:

- Ion channels reside in biological cell membranes, permitting ions to diffuse in or out of a cell (Sakmann & Neher, 1995). Power-law behavior characterizes various features of ion-channel behavior (Liebovitch, Fischbarg & Koniarek, 1987; Liebovitch, Fischbarg, Koniarek, Todorova & Wang, 1987; Liebovitch & Tóth, 1990; Liebovitch, Scheurle, Rusek & Zochowski, 2001; Läuger, 1988; Millhauser et al., 1988). Many ion channels exhibit independent power-law-distributed closed times between open times of negligible durations, and are well described by a fractal renewal point process (Lowen & Teich, 1993c). When the open times have significant duration, the alternating fractal renewal process serves as a suitable model instead (Lowen & Teich, 1993c, 1995; Thurner et al., 1997). Moreover, the time constant attendant to the recovery of certain ion channels depends on the duration of prior activity in a power-law fashion (Toib, Lyakhov & Marom, 1998).

- Fractal behavior exists in excitable-tissue recordings for various biological systems *in vivo*, from the microscopic to the macroscopic (Bassingthwaighte et al., 1994; West & Deering, 1994). Membrane voltages vary randomly in time, often exhibiting Gaussian fluctuations with power-law spectra (Verveen, 1960; Verveen & Derksen, 1968; Stern, Kincaid & Wilson, 1997; Lowen, Cash, Poo & Teich, 1997a). Superpositions of alternating fractal renewal processes, representing collections of ion-channel openings and closings, provide a plausible model for this process (Lowen & Teich, 1993d, 1995).

- Communication in the nervous system is generally mediated by the exocytosis of multiple vesicular packets (quanta) of neurotransmitter molecules at the synapse between cells, either spontaneously (Fatt & Katz, 1952) or in response to an action potential at the presynaptic cell (Katz, 1966). Neurotransmitter packets induce miniature end-plate currents (MEPCs) at the postsynaptic membrane, and their rate of flow exhibits fractal behavior such as power-law spectra, that can be described by a fractal-based point process (Lowen et al., 1997a,b).

- Power-law behavior characterizes the second-order statistics of action-potential sequences in isolated neuronal preparations and isolated axons; the spectrum often follows a form close to $1/f$ over a broad range of frequencies (Musha, Kosugi, Matsumoto & Suzuki, 1981; Musha et al., 1983). Moreover, the spike rate in response to a step-function input in many sensory neurons follows a power-law decay during the course of adaptation (Chapman & Smith, 1963), frequently varying as $t^{-1/4}$ (Biederman-Thorson & Thorson, 1971; Thorson & Biederman-Thorson, 1974).

- Auditory nerve-fiber action potentials from essentially all *in vivo* preparations display neural-spike clusters (Teich & Turcott, 1988) and fractal-rate behavior over time scales greater than about 1 sec, under both spontaneous and driven conditions (Teich, 1989; Teich, Johnson, Kumar & Turcott, 1990; Teich, 1992; Teich & Lowen, 1994; Lowen & Teich, 1992a, 1996a; Powers & Salvi, 1992; Kelly, Johnson, Delgutte & Cariani, 1996). This behavior could arise from superpositions of fractal ion-channel transitions (Teich, Lowen & Turcott, 1991; Lowen & Teich, 1993b, 1995) or via fractal-rate vesicular exocytosis (Lowen et al., 1997a,b).

- As in the auditory system, spontaneous and driven visual-system action potentials also exhibit fractal-rate characteristics. This behavior appears in all retinal ganglion cells and lateral-geniculate-nucleus cells in the thalamus (Teich et al., 1997; Lowen, Ozaki, Kaplan, Saleh & Teich, 2001), as well as in cells of the striate cortex (Teich et al., 1996). Moreover, insect visual-system interneurons generate spike trains with fractal-rate characteristics under both spontaneous and driven conditions (Turcott, Barker & Teich, 1995). Motion-sensitive neurons in the fly visual system adapt over a wide range of time scales that are established by the stimulus rather than by the neuron (Fairhall, Lewen, Bialek & de Ruyter van Steveninck, 2001a,b).

- Fractal features appear in action-potential sequences associated with many central-nervous-system neurons operating under a broad variety of conditions, including those in the cortex, thalamus, hippocampus, amygdala, pyramidal tract, medulla, and mesencephalic reticular formation (see, for example, Evarts, 1964; Yamamoto & Nakahama, 1983; Yamamoto, Nakahama, Shima, Kodama & Mushiake, 1986; Kodama, Mushiake, Shima, Nakahama & Yamamoto, 1989; Grüneis, Nakao, Yamamoto, Musha & Nakahama, 1989; Grüneis, Nakao, Mizutani, Yamamoto, Meesmann & Musha, 1993; Lewis, Gebber, Larsen & Barman, 2001; Orer, Das, Barman & Gebber, 2003; Fadel, Orer, Barman, Vongpatanasin, Victor & Gebber, 2004; Bhattacharya, Edwards, Mamelak & Schuman, 2005).

- Networks of rat cortical neurons contained in slice cultures exhibit brief neuronal avalanches whose spatiotemporal patterns are stable and repeatable for many hours; these power-law distributed structures may serve as a substrate for memory (Beggs & Plenz, 2003, 2004).

- Power-law behavior has a strong presence in the domain of sensory perception. Although the transduction of a stimulus at the first synapse in a neural system often follows a logarithmic form, stimulus estimation and detection are usually characterized by power-law functions of the stimulus intensity with sub-unity exponents (Stevens, 1957, 1971; Barlow, 1957; McGill & Goldberg, 1968; Moskowitz, Scharf & Stevens, 1974; McGill & Teich, 1995).

- The natural course of forgetting in humans is well described by a decaying power-law function of time (Wickelgren, 1977; Wixted & Ebbesen, 1991, 1997; Wixted, 2004).

There appear to be many origins of fractal activity in the nervous system; power-law fluctuations at the level of the protein may play an underlying role.

2.8.3 Fractals in medicine and human behavior

The quantitative analysis of the fractal characteristics of biomedical signals can yield information that assists with the diagnosis of disease and with the determination of its severity. This information, in turn, can have vital implications regarding the appropriate treatment regimen, and can influence the outcome of treatment. We provide a number of examples:

- Fractal analysis of the fluctuations in human standing (Musha, 1981; Shimizu et al., 2002) reveals age-related changes not evident using conventional, non-fractal methods (Collins et al., 1995). A different constellation of changes appears in Parkinson's disease (Mitchell, Collins, De Luca, Burrows & Lipsitz, 1995). After correcting for age, the fractal dynamics of human gait (walking) reveal the severity of Huntington's disease in patients, and appear to correlate with the degree of impairment (Hausdorff, Mitchell, Firtion, Peng, Cudkowicz, Wei & Goldberger, 1997).

- Fluctuations in mood show evidence of fractal behavior in their spectra, which display quantitative differences between bipolar-disorder patients and normal controls (Gottschalk et al., 1995). That these fluctuations follow a fractal form may lead to better methods for predicting and controlling mood disorders (see Sec. 2.8.5).

- Evidence of fractal behavior in the spectrum of the human heartbeat has been known for more than two decades (Kobayashi & Musha, 1982). Fractal methods do differentiate between normal and diseased patients with some degree of success (Turcott & Teich, 1993; Peng, Mietus, Hausdorff, Havlin, Stanley & Goldberger, 1993; Peng, Havlin, Stanley & Goldberger, 1995; Turcott & Teich, 1996). However, nonfractal measures (based on a fixed time scale of about twenty seconds) are superior for indicating the presence of cardiovascular dysfunction (Thurner, Feurstein & Teich, 1998; Thurner, Feurstein, Lowen

& Teich, 1998; Ashkenazy, Lewkowicz, Levitan, Moelgaard, Bloch Thomsen & Saermark, 1998; Teich et al., 2001).

- Fractal measures of activity have successfully quantified changes in the movement patterns of laboratory rats induced by drugs of abuse (Paulus & Geyer, 1992), and these same fractal measures help improve the diagnosis of attention deficit hyperactivity disorder (ADHD) in children (Teicher et al., 1996).

- Normal prenatal development may, in fact, require that fractal activity patterns be established in the brain. Developmental disorders such as autism could possibly result from a failure in the generation of these patterns (Anderson, 2001).

- Developmental insults, such as early abuse, quantitatively alter fractal parameters measured in experimental animals (Anderson, 2001). Evidence also exists that the fractal patterns of brain activity change with emotional state (Anderson et al., 1999), with implications for psychiatric diagnoses.

2.8.4 Recognizing the presence of fractal behavior

Fractal activity directly influences how systems operate. It is therefore important to recognize its presence, and to understand its features, so that system performance can be properly evaluated and controlled.

For computer network traffic (see Chapter 13) and vehicular traffic, for example, estimates of the fractal parameters provide measures of performance and useful design guidelines. Detailed analysis of fractal activity has proven to be indispensable. Dealing with fractal behavior in a system is not a trivial enterprise, however. Even seemingly simple tasks, such as calculating the mean and variance of the rate for a fractal process, offer unique challenges. The low-frequency nature of the noise indicates that nearby values are highly correlated so that obtaining reliable estimates often requires a prohibitive number of samples (see Chapter 12).

In some cases, fractal behavior serves as a source of unavoidable noise that diminishes system performance. An example is $1/f$-type noise in electronic components and circuits (see Sec. 5.4.1). The presence of fractal noise places restrictions on the information throughput of such systems, the calculation of which requires fractal analysis.

Finally, it is important to recognize the possible presence of fractal noise to avoid drawing erroneous conclusions. A case in point is the landmark study conducted by Fatt & Katz in 1952, in which the authors carried out an investigation of the statistical behavior of sequences of miniature endplate currents (MEPCs) at the neuromuscular junction. In the course of describing the methods used to analyze their data, they carefully noted that each segment of data selected for analysis was sufficiently short to exclude, as they put it, the "occasional occurrences of short high-rate bursts" of events, and to avoid "progressive changes of the mean." In fact, fractal-rate fluctuations

do exist in exocytic behavior and MEPCs (Lowen et al., 1997a,b), and the MEPCs observed by Fatt & Katz (1952) almost certainly exhibited such behavior (see Lowen et al., 1997b, for an analysis). Unaware of the presence or importance of these fluctuations, however, they removed most traces of them by selecting relatively short segments of data for analysis and, moreover, chose precisely those segments that exhibited minimal fluctuations. The observation of fractal-rate behavior requires long data sets, and the presence of both bursts and apparent trends lie at its very core.

2.8.5 Salutary features of fractal behavior

Fractal behavior is ubiquitous and its study reveals much about our surroundings. We discover, for example, that natural scenes and natural sounds exhibit fractal properties in space and time, and sensory systems have adapted to this property (Musha, 1981; Teich, 1989; Dan, Atick & Reid, 1996; Taylor, 2002; Simoncelli & Olshausen, 2001; Yu, Romero & Lee, 2005).

Given the ubiquity of fractal activity, what biological advantages might accrue from its presence?

Fractal behavior offers tolerance to noise and errors. The deleterious effects of noise diminish in importance because the concentration of power at lower frequencies assures increased predictability. New scales introduced by errors are less disruptive in fractal processes since they already exist in the initial distributions (West, 1990). Scale-free networks are robust against accidental failures, as pointed out in Sec. 2.7.8. Moreover, the presence of fractal noise can serve to optimize the throughput of a system, with examples in both neural signaling and vehicular traffic (Ruszczynski, Kish & Bezrukov, 2001).

Developmentally, internally generated fractal signals [such as neural signals arising during rapid-eye-movement (REM) sleep] provide a prenatal stimulus that mimics natural signals and assists the brain in developing normally. An animal can thus emerge at birth with its visual system attuned to the world it enters (Anderson, 2001). Search patterns executed by animals and by humans, which often have fractal properties (Cole, 1995; Viswanathan, Afanasyev, Buldyrev, Murphy, Prince & Stanley, 1996; Aks, Zelinsky & Sprott, 2002), appear optimal given the likely distributions of targets.

Finally, the salutary features of fractal behavior in medicine have been documented in a number of cases. When used for relieving pain via transcutaneous electrical nerve stimulation, $1/f$ noise outperforms white noise (Musha, 1981). This is also true for sensitizing baroreflex function in the human brain (Soma, Nozaki, Kwak & Yamamoto, 2003). The flexibility of response offered by fractal behavior may also serve as a harbinger of health (see West & Deering, 1995).

Problems

2.1 *Fractal and nonfractal objects* Comment on the fractal properties, or the lack thereof, in each of the following:

1. the aorta, all the arteries it branches into, the arterioles, and the capillaries in a rabbit;
2. a tree trunk and all its branches and twigs, as visualized in the winter when it is devoid of leaves;
3. a lock of hair;
4. a brick;
5. a sand dune in the Namibian desert, without vegetation;
6. a cumulus cloud;
7. the Himalayan mountains;
8. the path of a curve ball thrown by a major-league baseball pitcher;
9. a randomized version of $\mathcal{C}_3$ — we generate the third iteration towards the Cantor set, which contains eight segments, but add an independent random value uniformly distributed over $[-0.01, +0.01]$ to the beginning and ending value of each segment.

2.2 *Logistic to tent map* Consider the logistic map, Eq. (2.20), with $c = 4$, as studied in Sec. 2.6.2.

2.2.1. Show that the substitution

$$y \equiv \pi^{-1} \arccos(1 - 2x) \tag{2.31}$$

converts Eq. (2.20) into a tent map (Schroeder, 1990, p. 291):

$$y_{n+1} = \begin{cases} 2y_n & 0 \le y_n \le \frac{1}{2} \\ 2 - 2y_n & \frac{1}{2} < y_n \le 1. \end{cases} \tag{2.32}$$

2.2.2. Find the ratio $|\epsilon_{n+1}/\epsilon_n|$.

2.3 *Cantor variant* Imagine a variant of the Cantor set described in Sec. 2.4.1, denoted $\mathcal{C}'$. At each stage in the construction of the variant set we remove the middle *half* of each remaining interval. Thus, the intervals $\left[\frac{0}{4}, \frac{1}{4}\right] \bigcup \left[\frac{3}{4}, \frac{4}{4}\right]$ comprise the result $\mathcal{C}'_1$ after the first step in its construction.

2.3.1. What total length (Lebesgue measure) remains in the limiting set $\mathcal{C}'$?

2.3.2. How many points remain in $\mathcal{C}'$ compared with the original unit interval?

2.3.3. What value of D_0 does $\mathcal{C}'$ have?

2.4 *Cantor-set membership* Consider the point $x = 0.002002\ldots_3$, where the subscript $_3$ indicates a ternary expansion.

2.4.1. To what fraction does x correspond?

2.4.2. Does x belong to the endpoints of $\mathcal{C}$?

2.4.3. Does x belong to the interior of $\mathcal{C}$ (in other words, in $\mathcal{C}$ but not an endpoint of it)?

2.4.4. Does $\mathcal{C}$ contain irrational numbers?

2.5 *Scaling solution* Show that Eqs. (2.5) and (2.6) form the only solution to Eq. (2.4) for arbitrary a and x.